communications earth & environment

Article

A Nature Portfolio journal

https://doi.org/10.1038/s43247-026-04000-1

Episodic records of deep microbial methanogenesis throughout the Caledonian mountain range exhumation

Check for updates

Femke van Dam [1] ✉, Riikka Kietäväinen [2], George Westmeijer[3,4], Nick M. W. Roberts [5], Martin J. Whitehouse [6], Shuhei Ono [7], Jay Quade[8], Zhennan Wang [8], Thomas Wiersberg[9], Mark Dopson [1,3] & Henrik Drake [1]

The deep continental biosphere hosts microbial communities employing ancient metabolisms such as methanogenesis. Yet, it is one of Earth's least explored ecosystems with its long-term history remaining poorly constrained. This study integrated mineral, groundwater, and dissolved gas stable isotope analyses along with geochronological and previously published metagenomic data from the central Sweden 2276 m-deep COSC-2 borehole that intersects Silurian Caledonian thrust sheets and Precambrian basement. Extremely ^{13}C-enriched fracture-filling calcite ($\delta^{13}C$ up to + 28.9‰$_{V\text{-}PDB}$) indicated ancient microbial methanogenesis down to 1907 m depth. U–Pb dating revealed multiple episodes of ^{13}C-rich carbonate precipitation over hundreds of millions of years, including ages of 186 ± 20, 124 ± 20, 100 ± 22, 109 ± 17, 59 ± 4, and 1.8 ± 0.4 Ma along with a less certain age of 378 ± 65 Ma. Clumped-isotope temperatures decreased from ~70 to ~43 °C that reflected progressive exhumation. These results extend the temporal range of deep methanogenic biosignatures and demonstrate the resilience of subsurface life during long-term uplift and mountain range erosion.

The deep continental biosphere was posited by Gold[1] and since that time, it remains one of the least explored ecosystems on Earth. While its long-term evolutionary development remains poorly understood, it is proposed to hold clues to understanding evolution of life on Earth[2,3].

Methanogenesis, the process by which certain microorganisms produce methane, is believed to be over 3.5 billion years old[4]. Methanogenesis in the deep continental subsurface is a complex and vital process with significant implications for our understanding of adaptation and evolution of microbial life in extreme environments. This ancient metabolic process likely played a crucial role in shaping the early Earth's atmosphere and climate[5], making it a key component for understanding early Earth history and planetary bodies analogous to early Earth[6]. Methane-producing microorganisms, termed methanogens, are thought to have contributed to early global warming, which contributed to sufficiently warming the planet's surface to support liquid water despite the faint young Sun[7]. Recent studies have expanded our knowledge of methanogenesis in the deep subsurface. For instance, methanogenic archaea are documented in lithologically diverse deep bedrock environments with varying geological histories, such as in Fennoscandia, South Africa, and North America[8]. At Witwatersrand in South Africa, hydrogenotrophic methanogens are suggested to support the microbial community through syntrophic relationships[9]. In addition, Bomberg et al.[10] found methanogens at 572 m depth (Olkiluoto, Finland) that potentially use methylotrophic or hydrogenotrophic pathways, while acetoclastic methanogens are reported at 2260 m depth in Outokumpu, Finland[11]. These studies highlight the diversity and adaptability of methanogens in utilizing various substrates and survive under extreme energy limitation[12].

The Collisional Orogeny in the Scandinavian Caledonides (COSC) scientific drilling project aims to improve our understanding of Himalayan-type mountain-building processes by drilling two deep scientific boreholes in Jämtland, central Sweden. COSC-2 is a 2276 m deep cored borehole intersecting the Caledonian orogeny thrust sheets and its basement in central Sweden, formed by the underthrusting of the continent Laurentia by Baltica in the Silurian to early

[1]Centre for Environment (CENWIN), Linnaeus University, Kalmar, Sweden. [2]Department of Geosciences and Geography, University of Helsinki, Helsinki, Finland. [3]Centre for Ecology and Evolution in Microbial Model Systems (EEMiS), Linnaeus University, Kalmar, Sweden. [4]Department of Chemistry, Umeå University, Umeå, Sweden. [5]Geochronology and Tracers Facility, British Geological Survey, Nottingham, UK. [6]Department of Geosciences, Swedish Museum of Natural History, Stockholm, Sweden. [7]Department of Earth, Atmospheric, and Planetary Sciences, Massachusetts Institute of Technology, Cambridge, MA, USA. [8]Department of Geosciences, University of Arizona, Tucson, AZ, USA. [9]Geomechanics and Scientific Drilling, GFZ Helmholtz Centre for Geosciences, Potsdam, Germany. ✉e-mail: femke.vandam@lnu.se

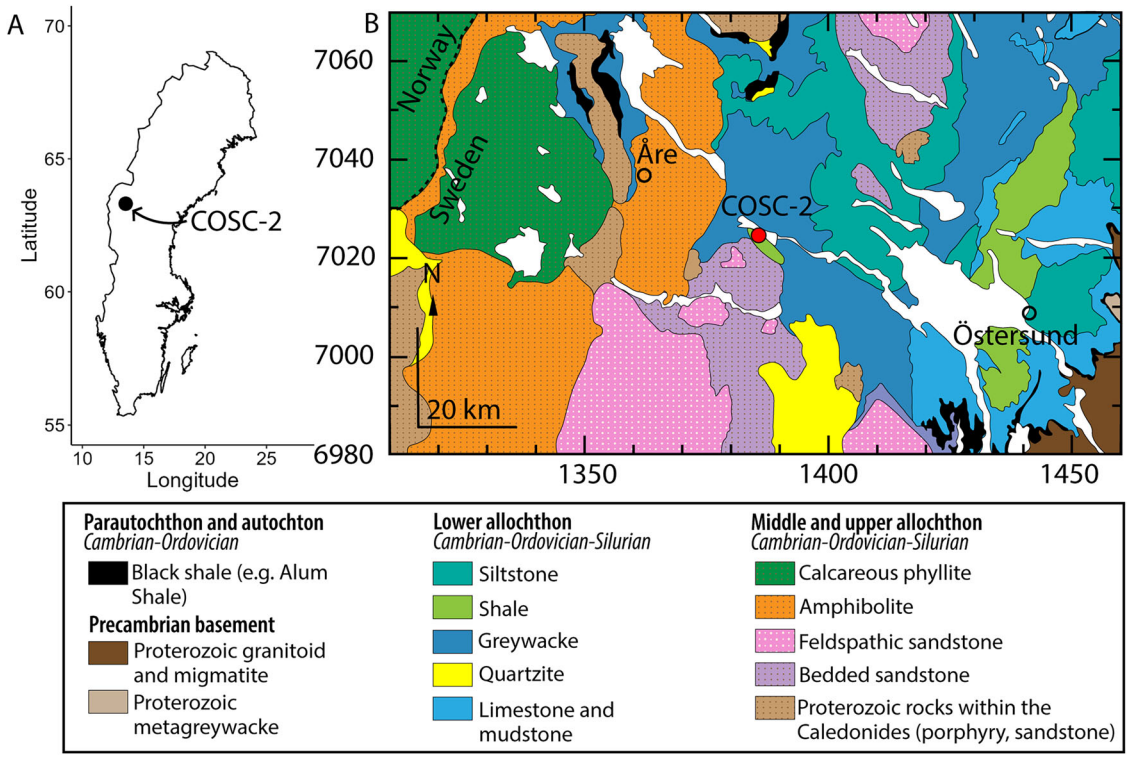


Fig. 1 | Location of the COSC-2 borehole. A Location of COSC-2, map in coordinate system WGS84 and **B** Geologic map redrawn from Korja et al.[78] after Karis and Strömberg[79], with coordinate system in RT90. Adapted with permission of Oxford University Press on behalf of the Royal Astronomical Society.

Devonian[13]. Post-orogeny, the area underwent rifting and denudation, resulting in exhumation[14]. Previous studies indicate that the groundwater system is an isolated aquifer containing a microbial community dominated by *Candidatus* Desulforudis audaxviator[15]. This species is an indicator for isolation and is proposed to have undergone only minimal evolution over hundreds of millions of years[16,17]. Moreover, *Ca.* Desulforudis audaxviator is one of four global deep groundwater populations, together with *Erythrobacter* sp., *Thiobacillus* sp., and lineages affiliated with the Methanobacteriaceae[18]. Therefore, the COSC-2 borehole (Fig. 1) is a key site to gain insights into subsurface microbial processes and their long-term habitation in a relatively isolated groundwater aquifer undergoing exhumation.

Here, we present a combined mineral, groundwater, and dissolved gas survey of biosignatures from COSC-2. The results suggested that methanogenic processes have been a persistent feature of the deep biosphere down to almost 2 km in this setting. U-Pb geochronology of calcite confirmed that microbial methanogenesis has been ongoing for up to >300 million years, providing a temporal framework for intermittent microbial methanogenesis at COSC-2. This long-term activity underscores the resilience and adaptability of microbial life in extreme environments, highlighting the extensive reach of subsurface life and contributes to our understanding of long-term igneous rock-hosted microbial methane formation.

Results

Mineralogy

The drill core was sampled for calcite- and/or pyrite-bearing open fractures from depths corresponding to those sampled for water and gas analysis. This includes the major conductive fracture (zone) of the thrust sheets at 975 m, that corresponds to the depth interval investigated for microbiological analyses[15]. Calcite varied between anhedral crystals as fine layers on the fracture wall (Fig. 2a, b) to subhedral-euhedral crystals (Fig. 2c) and pyrite was more rare (e.g. cubic in Fig. 2d). In total, three samples carried pyrite and 11 carried calcite. Other associated minerals included clay minerals, apophyllite, galena, marcasite, and zeolites.

Stable isotope compositions of calcite and pyrite

The $\delta^{13}C_{calcite}$ values from microscale secondary ion mass spectrometry (SIMS) analysis (n_{spots} = 105) ranged from −18.7 to 28.9‰ (V-PDB) over ten samples from varying depths (Fig. 3). The $\delta^{18}O_{calcite}$ values (n_{spots} = 108) ranged from −23.1 to −10.4‰$_{V\text{-}PDB}$ (Supplementary Data S1–S3). In the shallow samples (70, 100, 128, and 351 m depths), $\delta^{13}C_{calcite}$ ranged from −1.9 to 22.2‰$_{V\text{-}PDB}$ and the $\delta^{18}O_{calcite}$ ranged from −18.8 to −10.4‰ (V-PDB). These values were overall heavier compared to intermediate depth samples at the transition from sedimentary to crystalline lithology or deep samples in the crystalline basement. The intermediate depth samples (986–1270 m) had significant $\delta^{13}C_{calcite}$-variation, ranging from −18.7 to noteworthy ^{13}C-rich values of 28.9‰$_{V\text{-}PDB}$ at 1270 m depth, with relatively high $\delta^{18}O_{calcite}$ values (up to −11.1‰$_{V\text{-}PDB}$).

In the deep samples, $\delta^{13}C_{calcite}$ ranged from −8.7 to 17.5‰$_{V\text{-}PDB}$ and $\delta^{18}O_{calcite}$ ranged from −21.6 to −17.4‰ $_{V\text{-}PDB}$, with the sample at 1907 m depth being substantially ^{13}C-rich (up to 17.5‰$_{V\text{-}PDB}$). Overall, the calcite samples were homogeneous in composition (Fig. 4a), with little intra-crystal variability. The $\delta^{34}S_{pyrite}$ was measured in three samples (n_{spots} = 27; Supplementary Data S2) and varied from −3.8 to 39.1‰ (V-CDT), with the most notable ^{34}S-enrichment and range in values at 1204 m depth, which had an intra-crystal $\delta^{34}S_{pyrite}$ variability of up to 33‰ $_{V\text{-}CDT}$ (Fig. 4b).

Carbonate clumped isotope compositions of calcite

Due to small sample volumes in the deeper samples, the carbonate clumped isotope composition derived using laser spectroscopy was only acquired from calcite at shallow depth. The bulk values derived from the carbonate clumped isotope measurements generally overlapped with the SIMS data (Fig. 3). The temperatures derived from the carbonate clumped isotope measurements increased with depth with 42.7 ± 6.2, 52 ± 5, and

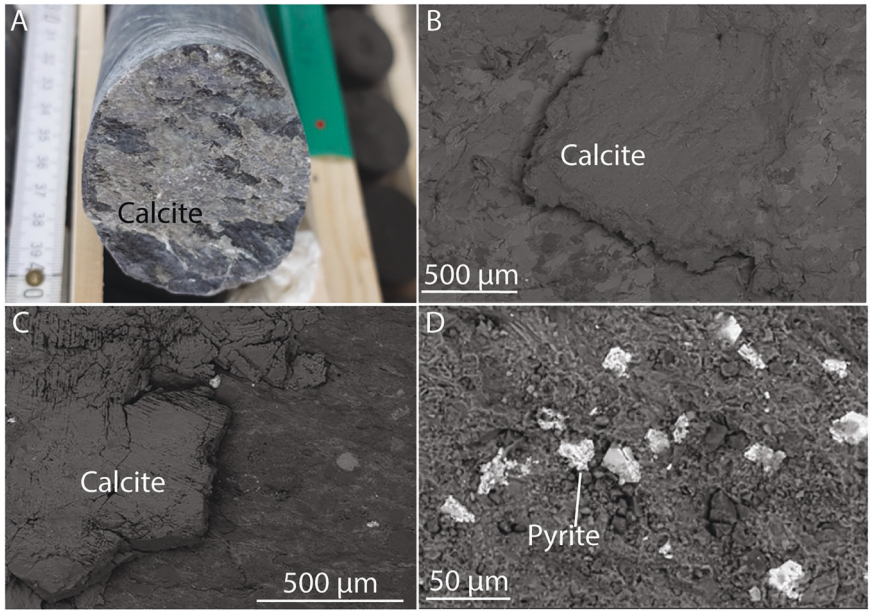


Fig. 2 | Secondary mineralogical features - calcite and pyrite. A Drill core fracture showing anhedral calcite crystals at 70 m; **B** Back-scattered (BSE-)SEM images of subhedral-euhedral calcite crystals from 1270 m depth; **C** BSE-SEM image of subhedral-euhedral calcite crystals from 100 m depth; and **D** BSE-SEM image of pyrite (BSE-bright) at 1204 m depth.

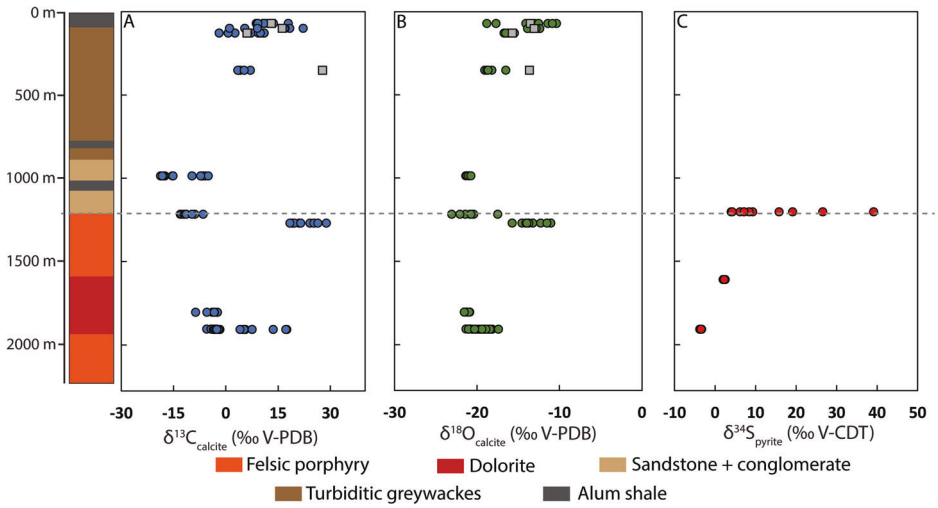


Fig. 3 | Isotopic composition of calcite and pyrite vs depth. A $\delta^{13}C_{calcite}$, **B** $\delta^{18}O_{calcite}$, **C** $\delta^{34}S_{pyrite}$. The gray line marks the contact between sedimentary rock and the crystalline basement. The colored symbols are from SIMS analysis, while the gray symbols are from carbonate-clumped isotope analysis. The simplified core description is from ref. 57.

69.6 ± 14 °C for the three samples at 70, 100, 128 m depth (Supplementary Data S4, S5). A temperature of 44.2 °C was derived from a single measurement from the sample at 351 m. From the reconstructed temperature and the $\delta^{18}O_{calcite}$, a paleo-fluid $\delta^{18}O_{H2O}$ composition was calculated using temperature-dependent $\delta^{18}O_{H2O\text{-}calcite}$ fractionation[19] (Supplementary Data S6). The paleo-$\delta^{18}O_{H2O}$ values ranged from −8.8 to −6.7‰ (V-SMOW).

U-Pb carbonate geochronology

The same calcite samples analyzed by SIMS were targeted for U-Pb geochronology using LA-ICP-MS (Fig. 5, Supplementary Fig. 1, Data S9, S10). At shallow depths, calcite provided dates of 109 ± 17 and 186 ± 20 Ma at 70 and 100 m depths, respectively (uncertainties at 2 σ). The outer zones of calcite from the 128 m depth sample produced an overlapping age of 124 ± 20 Ma, whereas the inner zones appeared to be older but did not provide a robust isochron (378 ± 65 Ma), indicating multiple episodes of calcite precipitation. Calcite samples at 351, 1270, and 1907 m depths provided dates of 59.4 ± 3.5, 1.82 ± 0.39, and 100 ± 22 Ma, respectively. In addition, calcite at 1217 m depth provided more scattered analyses indicating some possible disturbance of the U-Pb system, but with distinct outliers rejected an age of 342 ± 23 Ma was calculated. Finally, the 986 m sample yielded an age of 605 ± 27 Ma.

Groundwater and gas data

Gas and groundwater samples from 40 to 2081 m depth (sampling techniques described in Supplementary Text 1) gave relatively comparable gas compositions with the exception of the wellhead sample (0 m depth) that contained a large proportion of atmospheric air (Fig. 6A).

Methane concentrations varied between 49 to 90 % of total gas volume from 40 to 2081 m depth (Supplementary Table 1). N_2 was the second most abundant gas ranging from 6.42 to 39.8 %, ethane proportions ranged from 0.21 to 0.34 %, propane was below 0.026 %, and CO_2 was below detection (< 7 ppm) in most samples with a maximum of 0.01 % at 1907 m. In addition, The O_2 + Ar concentrations were not separated in the analysis, and their combined proportions were 0.5 to 8.4 % of total gas volume (Supplementary Table 3; Supplementary Text 2). Hydrogen was below detection (< 7 ppm) for most of the samples except at 810 and 1202 m where 0.12 and 0.091 % were detected. Finally, helium ranged from 0.8 to 3.5 %.

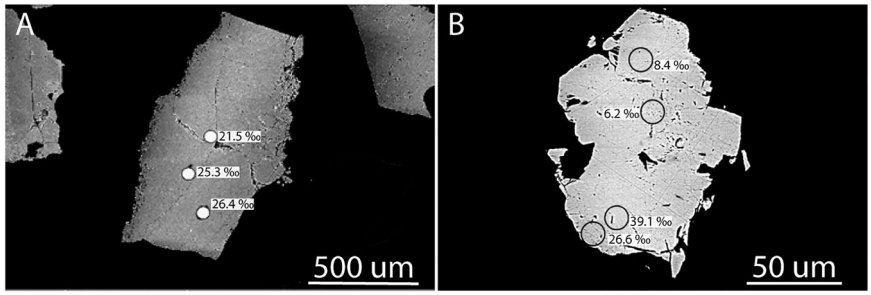


Fig. 4 | Minerals and stable isotope data. BSE-SEM images with SIMS spots. Calcite crystal from 1270 m with SIMS spots and $\delta^{13}C$ values marked (A) and a pyrite crystal from 1204 m with SIMS spots and $\delta^{34}S$ values (B).

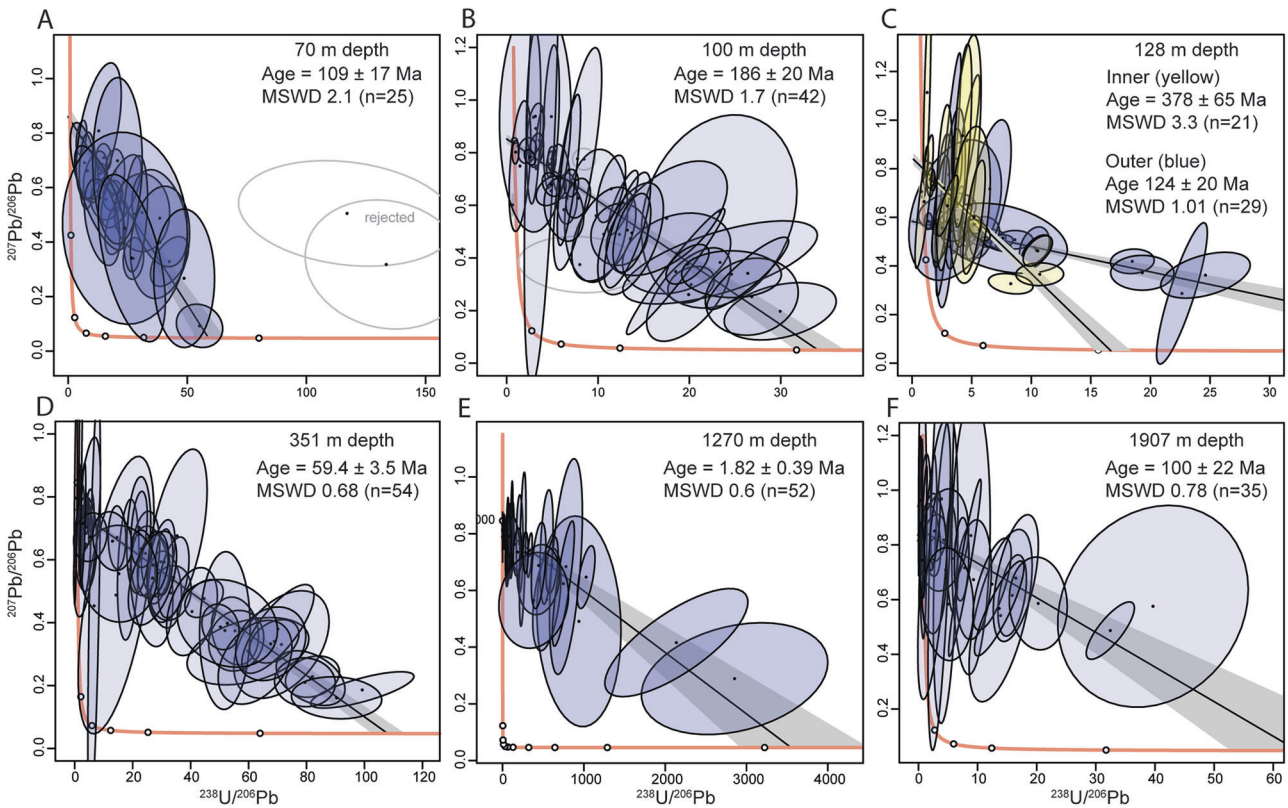


Fig. 5 | U-Pb carbonate geochronology. Samples **A** 70 m, **B** 100 m, **C** 128 m, **D** 351 m, **E** 1270 m, **F** 1907 m. Quoted ages reflect the lower intercept on a Tera-Wasserburg plot. Uncertainties are quoted at 2σ and include propagation of systematic uncertainties. Analytical data are reported in Supplementary Data S9.

The $\delta^{13}C_{CH4}$ values ranged from −35.1 to −27.0‰$_{V\text{-}PDB}$ and $\delta^{2}H_{CH4}$ from −324 to −287‰. Carbon isotope compositions of ethane ranged from −32.3 to −26.8‰$_{V\text{-}PDB}$ and $\delta^{13}C_{propane}$ values ranged from −29.5 to −25.4‰$_{V\text{-}PDB}$. Certain samples contained butane (*i*-C4 + *n*-C4) ranging from −26.1 to −23.5‰$_{V\text{-}PDB}$ for *i*-C4, and −26.1 to −24.3‰$_{V\text{-}PDB}$ for *n*-C4 (Fig. 6; Supplementary Table 2). Clumped isotopes of methane ($\Delta^{13}CH_3D$) at 975 m depth yielded 3.17 ± 0.21 (95 % confidence interval) giving an apparent temperature for methane formation or equilibration that was calculated to be 149 ± 15.5 °C. The stable isotope composition of water was analyzed over the depth interval 40-2081 m depth in the borehole (Supplementary Table 1), with $\delta^{18}O_{H2O}$ values ranging from −14.6 to −12.9‰$_{V\text{-}SMOW}$ and $\delta^{2}H_{H2O}$ values ranging from −89.3 to −83.7‰$_{V\text{-}SMOW}$ (Fig. 7 and Supplementary Table 2).

The values for SO_4^{2-} ranged from 40.2 to 104 mg L^{-1}, pH was between 8.2 to 9, and total dissolved solids (TDS) were 5600 to 12400 mg L^{-1}. Li concentrations varied from 2.2 to 3.5 mg L^{-1}, Br^- from 50.3 to 125, and Cl^- from 3489 to 7660 mg L^{-1}. The sample collected at 810 m had the lowest TDS, whereas the sample from 1905 m had the highest, although pumping prior to sampling at 1905 m likely reduced contributions from standing groundwater in the borehole (Supplementary Data S7).

Discussion

Microbial methanogenesis isotopically fractionates the substrate through preferential utilization of ^{12}C, resulting in the carbon substrate becoming ^{13}C-enriched and the methane ^{13}C-depleted[20]. This isotopic fractionation depends on the metabolic pathway utilized by the methanogen[21,22]. In autotrophic methanogenesis, CO_2 together with H_2 are converted into methane, leaving the remaining dissolved inorganic carbon (DIC) of the groundwater to become ^{13}C rich[23]. Subsequent reaction of the DIC (HCO_3^-) with dissolved Ca^{2+} results in precipitation of calcite, with isotopically heavy $\delta^{13}C$ signatures, making it a diagnostic tool for ancient microbial methanogenesis[24–27]. Acetoclastic methanogenesis can lead to enriched calcites as well. In this pathway, acetate that is produced from organic matter degradation becomes ^{13}C-enriched due to continuous fermentation[28,29]. The ^{13}C-enriched acetate is subsequently utilized by methanogens, producing ^{13}C-enriched CO_2 alongside CH_4, resulting in a ^{13}C rich inorganic carbon

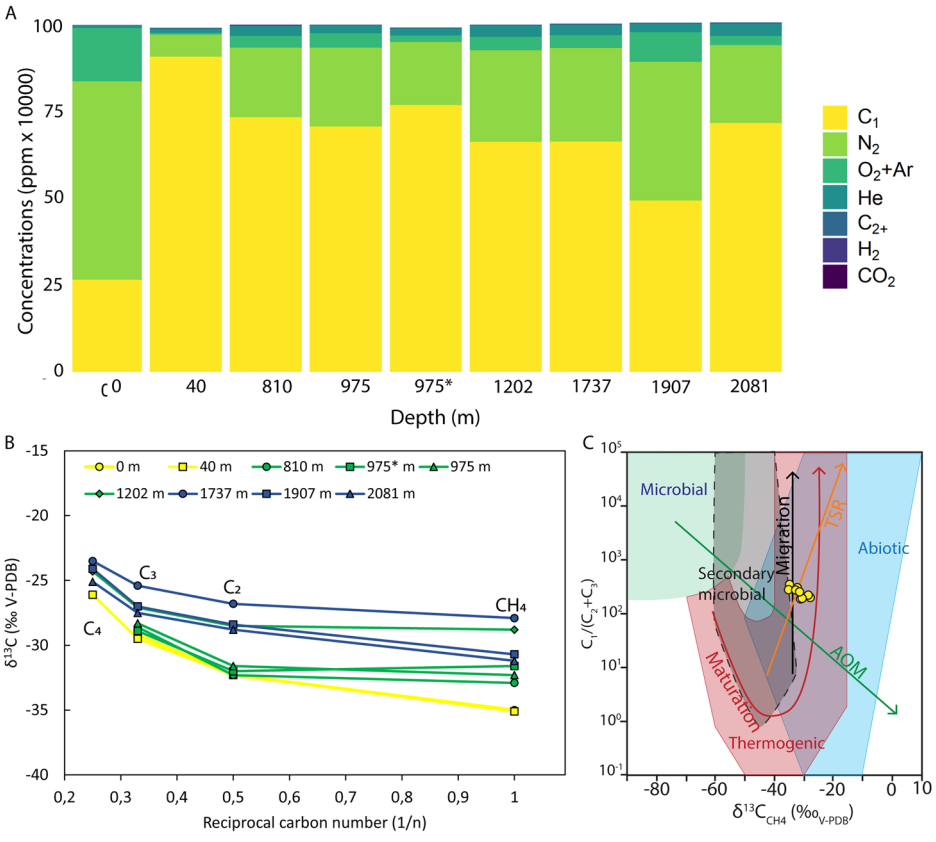


Fig. 6 | Gas characteristics. A Proportional gas compositions; **B** reciprocal carbon number and their carbon isotope compositions of the different hydrocarbons; and **C** $\delta^{13}C_{CH4}$ vs $C_1/C_2 + C_3$ modified after Milkov et al.[80]. AOM = anaerobic oxidation of methane and TSR = thermochemical sulfate reduction.

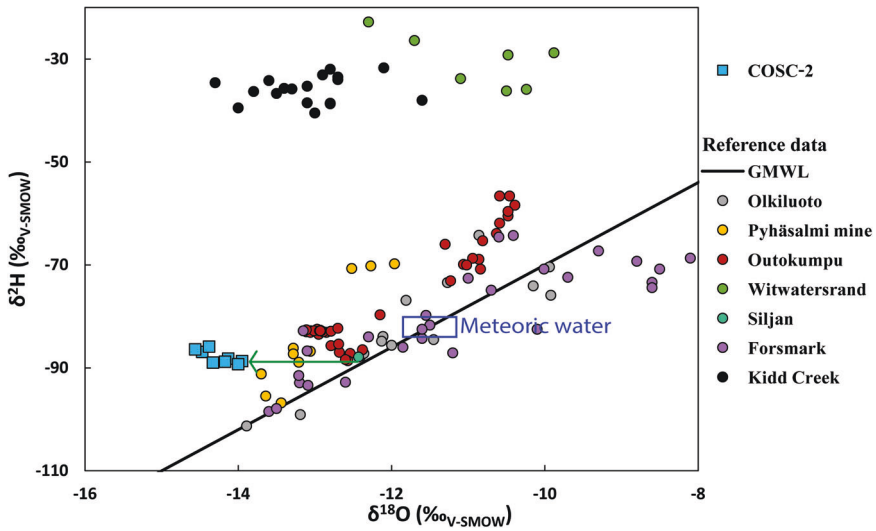


Fig. 7 | δ^2H and $\delta^{18}O$ of the groundwater. Reference data shown are from the Finland[81–83], Sweden[84,85], Kidd Creek[86–88] and Witwatersrand[89,90], excluding spots at >-8‰$_{V\text{-}SMOW}$ that are outside the graph. The box indicates meteoric recharge water[91] and the arrow indicates how the samples moved from the global meteoric water line (GMWL; Craig[92]).

pool. The significantly ^{13}C-enriched calcite crystals in this study of up to 28.9‰$_{V\text{-}PDB}$ (Fig. 3) thus support formation following microbial methane production, but the pathway is elusive (Fig. 8). The $\delta^{13}C$-rich calcite shows that microbial methanogenesis occurred in fractures from shallow to deep levels across nearly the entire studied sedimentary to crystalline bedrock profile. Organic carbon oxidation can result in $\delta^{13}C_{calcite}$ signatures around between -30 to -20‰$_{V\text{-}PDB}$[30], as organic matter has $\delta^{13}C$ values in this range. Depending on other (abiotic) carbon sources adding to the DIC pool, the resulting $\delta^{13}C_{calcite}$ value is slightly less negative than the microbial substrate, and the same applies for calcite formed via anaerobic oxidation of methane[31]. The calcite $\delta^{13}C$ value at 986 m depth indicated that the DIC of the precipitation fluids were depleted in ^{13}C, resulting in a relatively light $\delta^{13}C_{calcite}$ composition (mean -12‰$_{V\text{-}PDB}$) and indicate an influence of organic carbon oxidation (Fig. 8).

Pyrite can form abiotically following thermochemical sulfate reduction from hydrothermal fluids or microbial sulfate reduction. As the microbes utilize sulfate, their metabolism produces hydrogen sulfide typically strongly depleted in ^{34}S[32]. The hydrogen sulfide isotopic signature is transferred to the pyrite without significant fractionation[33], making $\delta^{34}S_{pyrite}$ a marker for microbial sulfate reduction. At deeper depths, the $\delta^{34}S_{pyrite}$ values ranged between -3.8 to 3.0‰$_{V\text{-}CDT}$. The dissolved sulfate in the modern groundwater at 975 m depth has a $\delta^{34}S_{sulfate}$ of 12.4‰$_{V\text{-}CDT}$[15]. Though the $\delta^{34}S_{sulfate}$ of the groundwater at the time of pyrite precipitation is unknown, assuming a similar isotopic composition of the dissolved sulfate at the time of precipitation of the pyrite, the enrichment factor $\varepsilon^{34}S$ ($\varepsilon^{34}S = \delta^{34}S_{sulfate} - \delta^{34}S_{pyrite}$)

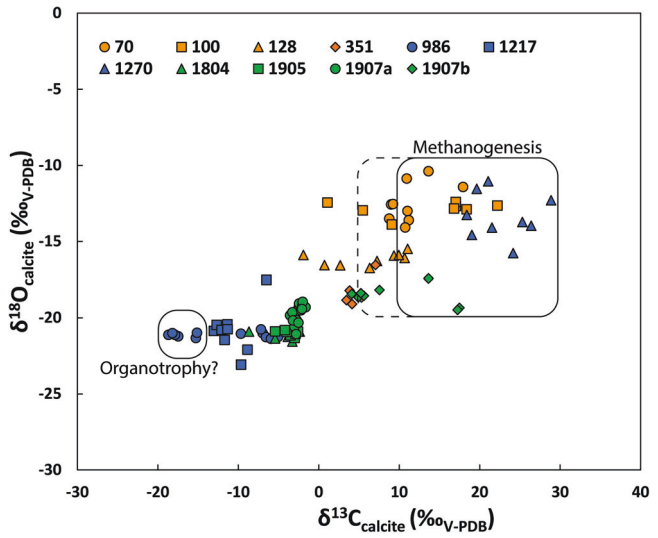


Fig. 8 | Stable isotope composition of calcite. $\delta^{13}C_{calcite}$ vs. $\delta^{18}O_{calcite}$ from SIMS analysis of calcite from shallow (orange), intermediate (blue), and deep depths (green). Fields for isotopic signatures represent different microbial processes: $\delta^{13}C_{calcite}$ > 10‰$_{V\text{-}PDB}$ methanogenesis; >5‰$_{V\text{-}PDB}$ dashed line; <−15‰ potential organotrophy. Fields are after Gustafsson et al.[37].

was between 9.4 to 16.2‰$_{V\text{-}CDT}$. However, $\varepsilon^{34}S$ overlaps with thermochemical sulfate reduction values and as fractionation factors for microbial sulfate reduction are typically above 20‰$_{V\text{-}CDT}$[34], it is not sole evidence for microbial sulfate reduction. Instead, this pyrite could have been hydrothermal pyrite, formed under high temperature. At intermediate depth the pyrite showed $\delta^{34}S$ values of up to 39.1‰$_{V\text{-}CDT}$. Enriched $\delta^{34}S_{pyrite}$ values can occur when the dissolved sulfate gradually becomes enriched in ^{34}S under closed system settings[35]. In a 'closed reservoir' system, the substrate is not replenished, and the sulfate pool is continuously depleted through microbial sulfate reduction. Meanwhile, the $\delta^{34}S_{SO4}$ becomes enriched and from this pool, ^{34}S-rich pyrite precipitates. The range of $\delta^{34}S$ of ~33‰$_{V\text{-}CDT}$ in a single pyrite crystal from this sample was also an indication of bacterial sulfate reduction as Rayleigh fractionation during bacterial sulfate reduction causes significant $\delta^{34}S_{sulfate}$ enrichment[36], a common feature in deep subsurface fracture systems[37–39]. Taken together, the mineral-infilling record provided several lines of support for ancient methanogenesis as well as microbial sulfate reduction in the fracture system.

The source of the groundwater and potential long-term water-rock interactions affect the isotope composition of water. The $\delta^{18}O_{H2O}$ deviation to the left of the global meteoric water line (Fig. 7) is typical for deep brines in crystalline basement[40]. Comparing the $\delta^{2}H_{H2O}$ and $\delta^{18}O_{H2O}$ results to other deep groundwaters, the composition was similar to the groundwater at Pyhäsalmi mine at depths between 2000-2400 m below surface level and the $\delta^{2}H_{H2O}$ values were similar to the groundwater at the Outokumpu borehole down to 1300 m[41]. Silicate hydrolysis and formation of clay minerals result in ^{18}O-depletion and ^{2}H-enrichment[40] and precipitation of calcite and zeolite may deplete the liquid phase in ^{18}O[42–44]. These mechanisms could explain the observed depleted $\delta^{18}O_{H2O}$ values, suggesting long-term water rock interaction in the studied groundwater samples.

For the shallow samples that have clumped isotope data, the calculated $\delta^{18}O_{paleofluid}$ was ^{18}O-enriched (-8.8 to -6.7‰$_{V\text{-}SMOW}$ (Supplementary Data S6) by 4 to 8‰$_{V\text{-}SMOW}$ compared to modern $\delta^{18}O_{H2O}$ (Fig. 7). This indicated a change over time in the groundwater composition and/or origin. The groundwater becoming less ^{18}O enriched can be due to water-rock interaction of the fluids over time, such as described above, or inflow of ^{18}O-depleted glacial meltwater.

The hydrogeochemical data indicated that the isolated 975 m fracture groundwater was saline (Cl^- 3700 mg L^{-1}) but non-marine, as the samples showed high Ca/Mg (4700-7000) and Br/Cl (~ 0.016) ratios, which is typical for deep saline waters and long-term water-rock-interaction[43]. There were variations in Cl^-, SO_4, Br, and Mg in the different samples over depth (Supplementary Data S7), indicating they were different waters or proportions of water types sampled over depth and/or different residence times of the groundwaters from different fractures. This also confirmed that samples at different depths represented inflow of different depth-resolved fractures.

Based on metagenomic and 16S ribosomal RNA gene sequencing, Westmeijer et al.[15] report a microbial community dominated by *Ca.* Desulforudis audaxviator. This species is a sulfate-reducing Bacillota and has been exclusively described in highly isolated, deep aquifers[16–18,45]. This further underscored that the groundwater in the sampled fractures represented an isolated, deep aquifer with very long residence times.

The methane isotopic composition did not provide compelling evidence for a microbial source and the reciprocal carbon number versus $\delta^{13}C$ did not give clear indications of biodegradation (Fig. 6B), such as preferential biodegradation of propane[46]. Instead, the gas isotopic compositions corresponded to thermogenic methane being the major source (Fig. 6C). Additional constraints on gas origin are provided by clumped isotopes of methane ($\Delta^{13}CH_3D$) as the temperature of the methane formation can be reconstructed if it is formed under thermodynamic equilibrium[47,48]. However, microbial methanogenesis typically reflects a disequilibrium signal, resulting in anomalously high apparent formation temperatures[49]. The $\Delta^{13}CH_3D$ yielded an apparent methane formation temperature of 149 ± 16 °C, far exceeding the modern temperature of ~25 °C[50]. This indicated that the methane had either migrated from greater depths, formed when temperatures were high, or formed under isotopic disequilibrium conditions, with the latter implying a microbial contribution to the methane pool.

In the 975 m depth fracture-hosted groundwater, a methanogen of the family Methanobacteriaceae is present with an abundance of <0.1 % of the read counts[15] with its reconstructed genome encoding hydrogenotrophic methanogenesis from CO_2 and H_2. H_2 was only detected at intermediate depths and at low concentrations, presumably due to active microbial consumption of H_2 and CO_2. Despite the presence of methanogens in the groundwater, the methane isotopic composition did not reflect a clear microbial signature. One gene involved in methanotrophy (*mmoC*; K16161) was encoded in reconstructed genomes of the orders Tissierellales and Saccharofermentanales, but no complete methanotrophic pathway was identified[15]. Therefore, the genomic evidence provides limited evidence for current microbial methanogenesis or methanotrophy occurring.

Fault and fracture reactivation can produce H_2, potentially supporting subsurface life[51,52] and can thus shape the microbial habitat[53]. While the gas samples did not indicate significant ongoing microbial methanogenesis, the calcite data provided a strong line of evidence for ancient microbial methanogenesis of episodic nature, occurring at different depths through time.

Apart from the sample 986 m that pre-dates the Caledonian orogeny and likely reflected paleo-karst precipitation in the sedimentary strata, the calcite ages (including those with isotopic composition reflecting methanogenic activity) postdated the Caledonian orogeny. In this study, the first indication of methanogenesis was Devonian, at ca. 378 Ma (large uncertainty), with the caveat that multiple zonation and two different ages were yielded for this sample (also 124 ± 20 Ma; Fig. 9). An age of 186 ± 20 Ma represented the first robust evidence of methanogenesis ($\delta^{13}C$ = 22.2‰$_{V\text{-}PDB}$) at a temperature of 52 ± 5 °C. Assuming a paleogeothermal gradient of 20 °C km^{-1} [50,54], and a Late Cretaceous average surface temperature of 15 °C, this would suggest approximately 1.7 km of denudation since the Early Jurassic and is supported by similar results of 42.7 ± 6 °C at 109 ± 17 Ma, suggesting a denudation of 1.3 km since the Late Cretaceous. The temperature of 69.6 ± 14 °C at 128 m would then correspond to a paleodepth of 2.6 km, although its age is unresolved (124 ± 20/378 ± 65 Ma), therefore a denudation estimate is uncertain. Indications for ancient methanogenesis go as deep as 1907 m in ^{13}C-rich calcite dated to 100 ± 22 Ma, corresponding to a paleodepth of approximately >3 km depth

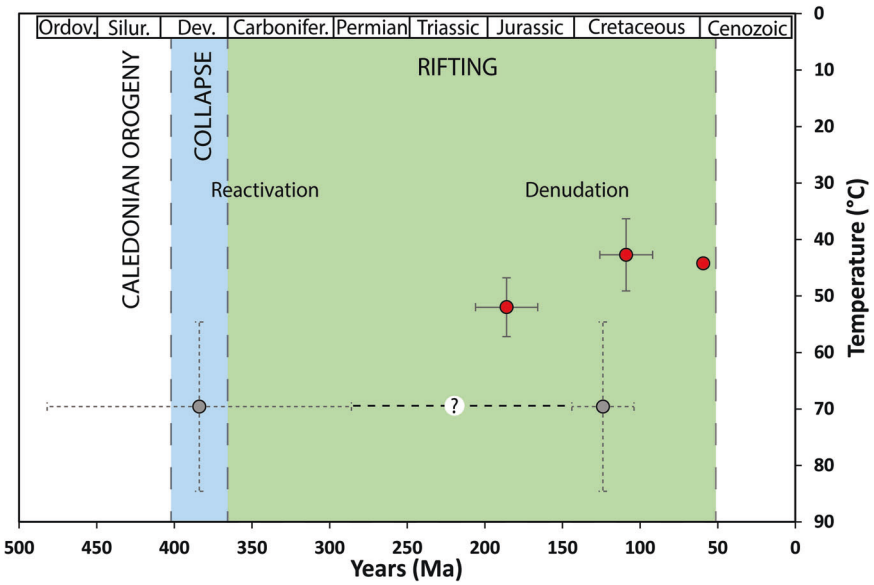


Fig. 9 | Paleotemperature from carbonate clumped isotope data vs. U-Pb ages. Geological context and timing of tectonic events from Peron-Pinvidic et al.[14].

given the aforementioned apparent denudation of at least 1.3 km since the Late Cretaceous, which is among the deepest ^{13}C-rich secondary calcite fracture-fills ever recorded[25]. These results show that ancient methanogenesis was a process not solely linked to near-surface fractures. Regional periods of extension causing fractures to form and/or re-open during exhumation have apparently allowed substrates and nutrients to circulate and infiltrate to great depth, creating opportunities for, and perhaps infiltration of, methanogens in the following regional geological context.

After the orogenic event, a phase of rifting initiated during the Late Devonian followed by reactivation during the Carboniferous that resulted in crustal thinning, hyperextension, exhumation, and re-activation of older structures[14]. Further time constraints on the reactivation phase have been mostly studied in southern Norway. For instance, based on palaeomagnetic studies, the Dalsfjord Fault underwent periods of brittle low-angle extensional reactivation during the Permian and Upper Jurassic/Lower Cretaceous (c. 150 Ma) that correspond to stages of major extensional movements on the continental shelf[55]. Early Cretaceous fault reactivation can be linked to North Sea or North Atlantic rifting[56], followed by a relatively tectonically stable period since 55 Ma. This stability has likely led to the present isolation of deep groundwaters as fractures have not been reopened, leading to a homogeneous gas composition with depth and no clear evidence of a microbial methane signature. However, this does not explain why the youngest dated calcite at 1270 m depth yielded an age of 1.82 ± 0.4 Ma. A possible explanation could be that the Late Cenozoic Ice Age beginning around 2.6 Ma with ice sheets loading and unloading the crust may have induced minor fracturing events and fluid circulation, potentially linking the microbial activity linked to late-stage fracture reactivation. Although no evidence of glacial meltwater penetrating to this depth was recorded in the calcite mineral, the sample occurs directly below the Caledonian décollement, which may be a zone of weakness susceptible to reactivated after a long period of stability. This young calcite age at this depth therefore suggests that water infiltration within the fracture network has been heterogeneous through time, with different flow paths becoming active at different times.

Taken together, deep methanogenesis in this system appeared to be episodic rather than continuous, varying with depth and time. This pattern was potentially caused by short-lived windows of enhanced permeability allowing substrate flow and was not necessarily linked to major tectonic events. Isotopic evidence of hundreds of million-year-old microbial methanogenesis was found throughout the borehole, to notable depths of 1907 m. These findings are among the deepest ^{13}C-rich secondary calcite fracture-fills ever recorded and indicate how microbial activity was stimulated by fracture-reactivation and fluid mixing events during progressive exhumation of the mountain range. This has implications for the resilience of life in the deep biosphere in general and microbial methanogenesis in particular. Geological processes such as denudation and fault reactivation could be essential for facilitating deep subsurface methanogenesis. It also shows that a combination of proxies for methanogenesis such as gas compositions, microbial communities, and isotopic inventories of secondary minerals gives a holistic view of how microbial activity varies over time.

Methods

Study site

The COSC-2 borehole is located in central Sweden (63.3124° N, 13.5259° E) at an elevation of 320 m with a depth of 2276 m from the surface[50]. The basement is at ~1215 m depth of the core, consisting of felsic porphyry aged 1.66-1.65 Ga[57,58] intruded by dolerite dykes (1.47 Ga and 1.27-1.26 Ga;[59,60]). Overlaying the basement is a sedimentary sequence of conglomerates and heterogeneous sediments, which is covered by sandstone turbidites and shales (alum shale formation[57]).

The Caledonides of western Scandinavia were formed during collisional orogenesis resulting from ocean opening during the Cambrian, development of intra-oceanic and arc-continent subductions systems during the Ordovician, and underthrusting of the continent Laurentia by Baltica in the Silurian to early Devonian[13]. This caused emplacement of allochthonous nappes for several hundreds of kilometers. The uppermost part of the borehole consists of Ordovician turbidites, underlain by the Lower Allochthon, the deeper Cambro-Ordovician sedimentary rocks, and crystalline Precambrian basement. The Caledonian orogeny at ca. 490–390 Ma was the last collisional event with the area being tectonically stable since the North Atlantic break-up at ~55 Ma[61,62].

Sampling

Seven 0.6 L fluid samples were collected from different depths of the COSC-2 borehole using a Leutert Positive Displacement Sampler (PDS). The sampler was lowered into the borehole on a four-conductor logging cable and opened at the target depth by a trigger signal from the surface. Once opened, fluid entered the sampler under the elevated pressure of the borehole fluid column, continuously expanding the sampling volume. This technique allowed sampling under constant pressure and minimizes e.g., uncontrolled degassing. After 0.6 L of fluid had entered the sampler, the inlet valve was closed from the surface and the sampler retrieved under in situ

pressure conditions. At the surface, the sample was transferred into a steel cylinder while maintaining in situ pressure. In a field laboratory, the fluid was then transferred into a glass apparatus with a defined volume for phase separation and subsampling of gas and water. Details on the sampling process, sample transfer, and fluid separation into gas and water phases are provided in Regenspurg et al.[63] and Feldbush et al.[64]. At 975 m depth the sampling was later repeated using packers and a pressurized in situ sampling device (PAKO) as described in Westmeijer et al.[15] and Supplementary Text 1. Pump samples were also taken from 40 m depth and spontaneously separated gas collected at the wellhead.

Gas compositions

Gas samples were analyzed by Applied Petroleum Technology (APT), Oslo, Norway for full chemical and isotope compositions (Supplementary Tables 1 and 2). Hydrocarbons were identified and quantified with an Agilent 7890 A Gas Chromatograph (GC) equipped with a flame ionization detector (FID) and H_2, CO_2, N_2, and O_2 + Ar with a thermal conductivity detector using an HP PONA chromatographic column (50 m length, 0.2 mm internal diameter, 0.5 µm film thickness). The temperature program of the GC-oven started at 30 °C for 10 min followed by heating to 60 °C (held for 10 min) with 2 °C min^{-1}, heating to 130 °C with 2 °C min^{-1}, and heating to 320 °C (held for 25 min) with 4 °C min^{-1}. 2,2,4-tri-methylpentane was used as an internal standard. The stable carbon isotopic composition of the hydrocarbon components in the gas was determined by a GC coupled to a combustion and isotope ratio mass spectrometer (IRMS), with a reproducibility of $\delta^{13}C$ values better than 1‰$_{V\text{-}PDB}$ (2 sigma). The methane hydrogen isotope composition was determined with a reproducibility of δD values better than 10‰$_{V\text{-}SMOW}$ (2 sigma).

Free gas methane-clumped isotopologues were measured at the Massachusetts Institute of Technology, Cambridge, USA. The methane was extracted and purified following the preparative GC method described by Wang et al.[49]. The relative abundances of methane isotopologues $^{12}CH_4$, $^{13}CH_4$, $^{12}CH_3D$, and $^{13}CH_3D$ were measured using a tunable infrared laser direct absorption spectroscopy (TILDAS) as previously described in Ono et al.[65]. TILDAS values of $\delta^{13}C$ and δD of methane were calibrated via measurements of natural gas standards NGS-1 and NGS-3[49]. The abundance of $^{13}CH_3D$ isotopologue was reported as $\Delta^{13}CH_3D$, a metric representing the deviation of the abundance of $^{13}CH_3D$ from a stochastic distribution of isotopes among isotopologues $^{12}CH_4$, $^{13}CH_4$, $^{12}CH_3D$, and $^{13}CH_3D$ according to Eq. (1).

$$\Delta^{13}CH_3D = \frac{\left[13_{CH_3D}\right]\left[12_{CH_4}\right]}{\left[13_{CH_4}\right]\left[12_{CH_3D}\right]} - 1 \quad (1)$$

The stochastic isotopologue ratios (i.e., $\Delta^{13}CH_3D = 0$) were determined by thermally equilibrating methane at 250 °C using a Pt catalyst[65] and theoretical fractionation factors[66].

Mineral sampling and SEM

Thirteen rock core intervals containing open, partly sealed, or completely sealed fractures and vugs were targeted and sampled for secondary minerals coatings, focusing on calcite and pyrite. The crystals were characterized under a stereomicroscope and identified directly on the uncoated surfaces of fractures using a FEI Quanta 650 FEG scanning electron microscope (SEM) equipped with an integrated energy dispersive spectroscopy (EDS). SEM-EDS analyses were performed in low vacuum to minimize surficial charging effects which enable the use of uncoated samples. The acceleration voltage was 20 kV and the instrument was calibrated with a cobalt standard.

SIMS

Following sample characterization and mineral identification, single crystals or aggregates were carefully separated from fractures and vugs with a chisel and/or tweezers under a stereomicroscope and then mounted in epoxy. The epoxy mounted grains were polished to expose crystal cross-sections and characterized in SEM once again to identify crystal zonation, cracks, mineral inclusions, and impurities to optimize spot placement prior to SIMS analysis. Intra-crystal SIMS-analysis (10 µm lateral beam dimension, 1-2 µm depth dimension) of carbon, oxygen, and sulfur isotopes were performed on a CAMECA IMS1280 SIMS at NordSIMS, Swedish Museum of Natural History, Stockholm, Sweden.

Calcite

Analytical transects were made within calcite crystals extracted from 11 drill core intervals. In total, 213 analyses were made, 105 for $\delta^{13}C$ and 108 for $\delta^{18}O$ using previously described settings[67]. Influence of organic matter and inclusions of other minerals was avoided by careful spot placement to areas in the crystals without microfractures or inclusions. The uncertainty associated with potential organic inclusions and matrix composition was therefore considered to be insignificant compared to the isotopic variations. Calcite results were reported as‰ $\delta^{13}C$ and $\delta^{18}O$ based on the Pee Dee Belemnite (V-PDB)-standard value. Analytical sessions were carried out by running blocks of six unknowns bracketed by two standards. Spot transects were made from core to rim within the crystals (full data including standard values in Supplementary Data S1 and S2). Corresponding analytical spots for C and O isotopes were closely placed within the crystals and analyzed during separate sessions. Isotope data were normalized using calcite reference material S0161, which comes from a granulite facies marble in the Adirondack Mountains, courtesy of R.A. Stern (University of Alberta, Canada). The values used for instrumental mass fractionation correction were determined by conventional stable isotope mass spectrometry at Stockholm University, Sweden on ten separate pieces, yielding $\delta^{13}C$ = -0.22 ± 0.11‰ V-PDB (1 std. dev.) and $\delta^{18}O$ = -5.62 ± 0.11‰ V-PDB (1 std. dev.). Precision was $\delta^{18}O$: ± 0.2-0.3‰ and $\delta^{13}C$: ± 0.4-0.5‰.

Pyrite

Analytical transects were made from core to rim within pyrite crystals from three drill core samples. In total, 27 analyses were made for $\delta^{34}S$. Sulfur was sputtered using a $^{133}Cs^+$ primary beam with 20 kV incident energy (10 kV primary, -10 kV secondary) and a primary beam current of ~1.5 nA. A normal incidence electron gun was used for charge compensation. Analyses were performed in automated sequences, with each analysis comprising a 70 s pre-sputter to remove the gold coating over a rastered 15 × 15 µm area, centering of the secondary beam in the field aperture to correct for small variations in surface relief and data acquisition in sixteen four second integration cycles. The magnetic field was locked at the beginning of the session using a nuclear magnetic resonance field sensor. Secondary ion signals for ^{32}S and ^{34}S were detected simultaneously using two Faraday detectors with a common mass resolution of 4860 (M/ΔM). Results (n = 27) were reported as‰ $\delta^{34}S$ based on the Canyon Diablo Troilite (V-CDT)-standard value[68].

LA-ICP-MS U-Pb carbonate geochronology

Calcite crystals previously analyzed for SIMS C-O were dated with Laser Ablation Inductively Coupled Plasma Mass Spectrometry at the Geochronology and Tracers Facility, British Geological Survey, Nottingham, UK. The method follows that described previously (e.g.,[27]) utilizing an Elemental Scientific Lasers 193 nm ImageGeo system fitted with a TV3 cell, coupled to a Nu Instruments Attom single collector ICP-MS run in peak-hopping mode. Standard-sample-bracketing comprised a homogeneous material for normalization of Pb/Pb ratios (zircon 91500, NIST612, or NIST614 depending on session) and a matrix-matched reference material for normalization of U-Pb ratios (WC1[69]; or RA138[70]). Secondary reference materials were run for validation, including RA138[70] and Duff Brown[71]. All analytical results and the analytical conditions are provided in Supplementary data S8-S10.

Clumped isotopes of calcite

For clumped isotope of calcite analysis ($n = 4$), about 2 mg of powdered carbonate was reacted with dehydrated phosphoric acid under vacuum at 70 °C. The conventional isotope ratio measurement relative to V-PDB was calibrated based on repeated measurements of International Atomic Energy Agency (IAEA) reference materials. Carbonate-clumped isotope values ($\Delta^{16}O^{13}C^{18}O$, Δ638) are reported in the Intercarb-Carbon Dioxide Equilibrium Scale (I-CDES) reference frame defined by ETH 1–4 carbonate standards and Carbon Dioxide Equilibrium Scale (CDES) reference frame defined by water-equilibrated gases and heated gases[72,73]. The Δ638 notation referred to measurements using a tunable infrared laser differential spectrometer (TILDAS), performed at the Environmental Isotope Laboratory at the University of Arizona, USA. The precision values for these measurements were ± 0.021‰ for Δ638, ± 0.04‰ for $\delta^{18}O_{carb}$, and ± 0.03‰ for $\delta^{13}C_{carb}$ (pooled reproducibility[74], 1σ). The laser-based Δ638–temperature relationship for carbonates at relatively low temperatures was based on 44 synthetic calcites that equilibrated at temperatures from 6 to 70 °C[75] according to Eq. (2).

$$\Delta 638\mathrm{CDES} = (0.0405 \pm 0.0006) \times (106/\mathrm{T2}) + (0.1822 \pm 0.0061),\ \mathrm{R2} = 0.985 \quad (2)$$

Temperature estimates using laser-based Δ638 and mass spectrometry-based Δ47 measurements are statistically equivalent[75]. Equation (2) was within error of recent mass spectrometry-based Δ47-temperature relationships and correctly predicted precipitation temperatures for a suite of 17 natural carbonates for both calcite and aragonite[75]. Complete details of this method and the calibration of the Δ638–temperature relationships are described in Roberts et al.[76] and Wang et al.[77].

Hydrogeochemistry

Trace elements and major cation analyses of the PDS samples were performed at the ElMiE Lab at the GFZ Helmholtz Centre for Geosciences, Potsdam, Germany. Fluid samples were diluted with 2 vol.% HNO_3 and doped with 1 μL L^{-1} In to correct for instrumental mass drift. The trace elements were measured using high resolution inductively coupled plasma mass spectrometry (ICP-MS; ELEMENT 2XR, Thermo Scientific, Waltham, USA). Repeatability was within 15 % determined based on repeated analysis of individual samples. The acid blank was subtracted from each measurement. Major cations were analyzed by ICP coupled with optical emission spectroscopy using a 5110 spectrometer with Vertical Dual View configuration (Agilent, USA). The analytical precision and repeatability were generally better than 5 % and are regularly tested by certified reference material and in-house standards.

Water stable isotopes

Water stable isotope composition ($\delta^{18}O$ and $\delta^{2}H$) of filtered (< 0.45 μm) water samples were analyzed at the Geological Survey of Finland in Espoo, Finland (PAKO and pump samples) and at the Hellabs Environmental laboratories at the University of Helsinki, Finland (PDS samples) using cavity ring-down spectroscopy (CRDS, Picarro Inc., USA), and reported in ‰ against the Vienna Standard Mean Ocean Water reference (V-SMOW). V-SMOW and V-SLAP (Vienna Standard Light Antarctic Precipitation) calibrated standards were analyzed between the samples to calibrate the measurements. Precision was ± 0.15‰ for oxygen and ± 1‰ for hydrogen.

Data availability

All data used in this manuscript are included in the published article and supplementary data files. All data files have been uploaded to Swedish National Data Service (www.snd.se; https://doi.org/10.5878/3e25-9238). Supplementary data files contain all isotopic and automated mineralogy data used to generate the figures.

Received: 13 February 2026; Accepted: 21 August 2026;
Published online: 01 September 2026

References

1. Gold, T. The deep, hot biosphere. *Proc. Natl. Acad. Sci.* **89**, 6045–6049 (1992).
2. Ivarsson, M. et al. The fossil record of igneous rock. *Earth. Sci. Rev.* **210**, 103342 (2020).
3. McMahon, S. & Ivarsson, M. A new frontier for palaeobiology: Earth's vast deep biosphere. *BioEssays* **41**, 1900052 (2019).
4. Wolfe, J. M. & Fournier, G. P. Horizontal gene transfer constrains the timing of methanogen evolution. *Nat. Ecol. Evol.* **2**, 897–903 (2018).
5. Sauterey, B., Charnay, B., Affholder, A., Mazevet, S. & Ferrière, R. Co-evolution of primitive methane-cycling ecosystems and early Earth's atmosphere and climate. *Nat. Commun.* **11**, 2705 (2020).
6. Glass, J. B. & Hörst, S. M. The once and future gas: methane's multifunctional roles in Earth's evolution and potential as a biosignature. *Annu. Rev. Earth Planet. Sci.* **53**, 283–304 (2025).
7. Charnay, B. et al. Exploring the faint young Sun problem and the possible climates of the Archean Earth with a 3-D GCM. *J. Geophys. Res. Atmos.* **118**, 10414–10431 (2013).
8. Kietäväinen, R. & Purkamo, L. The origin, source, and cycling of methane in deep crystalline rock biosphere. *Front. Microbiol.* **6**, 725 (2015).
9. Lau, M. C. Y. et al. An oligotrophic deep-subsurface community dependent on syntrophy is dominated by sulfur-driven autotrophic denitrifiers. *Proc. Natl. Acad. Sci.* **113**, E7927–E7936 (2016).
10. Bomberg, M., Lamminmäki, T. & Itävaara, M. Microbial communities and their predicted metabolic characteristics in deep fracture groundwaters of the crystalline bedrock at Olkiluoto, Finland. *Biogeosciences* **13**, 6031–6047 (2016).
11. Nuppunen-Puputti, M. et al. Rare biosphere archaea assimilate acetate in the Precambrian terrestrial subsurface at 2.2 km depth. *Geoscience* **8**, 418 (2018).
12. Escudero, C., Oggerin, M. & Amils, R. The deep continental subsurface: the dark biosphere. *Int. Microbiol.* **21**, 3–14 (2018).
13. Gee, D. G., Juhlin, C., Pascal, C. & Robinson, P. Collisional Orogeny in the Scandinavian Caledonides (COSC). *GFF* **132**, 29–44 (2010).
14. Peron-Pinvidic, G. & Osmundsen, P. T. From orogeny to rifting: insights from the Norwegian 'reactivation phase'. *Sci. Rep.* **10**, 1–8 (2020).
15. Westmeijer, G. et al. *Candidatus* Desulforudis audaxviator dominates a 975 m deep groundwater community in central Sweden. *Commun. Biol.* **7**, 1–10 (2024).
16. Becraft, E. D. et al. Evolutionary stasis of a deep subsurface microbial lineage. *ISME J.* **15**, 2830–2842 (2021).
17. Karnachuk, O. V. et al. Domestication of previously uncultivated *Candidatus* Desulforudis audaxviator from a deep aquifer in Siberia sheds light on its physiology and evolution. *ISME J.* **13**, 1947–1959 (2019).
18. González-Rosales, C. et al. A global deep terrestrial biosphere core microbiome. *ISME Commun.* **5**, 1–15 (2025).
19. O'Neil, J. R., Clayton, R. N. & Mayeda, T. K. Oxygen isotope fractionation in divalent metal carbonates. *J. Chem. Phys.* **51**, 5547–5558 (1969).
20. Whiticar, M. J. Carbon and hydrogen isotope systematics of bacterial formation and oxidation of methane. *Chem. Geol.* **161**, 291–314 (1999).
21. Kinnaman, F. S., Valentine, D. L. & Tyler, S. C. Carbon and hydrogen isotope fractionation associated with the aerobic microbial oxidation of methane, ethane, propane and butane. *Geochim. Cosmochim. Acta* **71**, 271–283 (2007).
22. Penger, J., Conrad, R. & Blaser, M. Stable carbon isotope fractionation by methylotrophic methanogenic archaea. *Appl. Environ. Microbiol.* **78**, 7596–7602 (2012).
23. Boehme, S. E., Blair, N. E., Jeffrey Chanton, L. P. & Martens, C. S. A mass balance of ^{13}C and ^{12}C in an organic-rich methane-producing marine sediment. *Geochim. Cosmochim. Acta* **60**, 3835–3848 (1996).

24. Irwin, H., Curtis, C. & Coleman, M. Isotopic evidence for source of diagenetic carbonates formed during burial of organic-rich sediments. *Nature* **269**, 209–213 (1977).
25. Liu, W. et al. ^{13}C-enriched carbonate precipitates reveal intense methanogenic oil degradation in the upper Wuerhe Formation, Northwest China. *Geology* **52**, 830–835 (2024).
26. Budai, J. M., Martini, A. M., Walter, L. M. & Ku, T. C. W. Fracture-fill calcite as a record of microbial methanogenesis and fluid migration: a case study from the Devonian Antrim Shale, Michigan Basin. *Geofluids* **2**, 163–183 (2002).
27. Drake, H. et al. Isotopic evidence for microbial production and consumption of methane in the upper continental crust throughout the Phanerozoic eon. *Earth Planet. Sci. Lett.* **470**, 108–118 (2017).
28. Dimitrakopoulos, R. & Muehlenbachs, K. Biodegradation of petroleum as a source of 13C-enriched carbon dioxide in the formation of carbonate cement. *Chem. Geol. Isot. Geosci. Sect.* **65**, 283–291 (1987).
29. Franks, S. G. et al. Carbon isotopic composition of organic acids in oil field waters, San Joaquin Basin, California, USA. *Geochim. Cosmochim. Acta* **65**, 1301–1310 (2001).
30. Sahlstedt, E., Karhu, J. A. & Pitkänen, P. Indications for the past redox environments in deep groundwaters from the isotopic composition of carbon and oxygen in fracture calcite, Olkiluoto, SW Finland. *Isot. Environ. Health Stud.* **46**, 370–391 (2010).
31. Peckmann, J. & Thiel, V. Carbon cycling at ancient methane–seeps. *Chem. Geol.* **205**, 443–467 (2004).
32. Chambers, L. A. & Trudinger, P. A. Microbiological fractionation of stable sulfur isotopes: a review and critique. *Geomicrobiol. J.* **1**, 249–293 (1979).
33. Böttcher, M. E., Smock, A. M. & Cypionka, H. Sulfur isotope fractionation during experimental precipitation of iron(II) and manganese(II) sulfide at room temperature. *Chem. Geol.* **146**, 127–134 (1998).
34. Machel, H. G., Krouse, H. R. & Sassen, R. Products and distinguishing criteria of bacterial and thermochemical sulfate reduction. *Appl. Geochem.* **10**, 373–389 (1995).
35. Seal, R. R. Sulfur isotope geochemistry of sulfide minerals. *Rev. Mineral. Geochem.* **61**, 633–677 (2006).
36. Riciputi, L. R., Cole, D. R. & Machel, H. G. Sulfide formation in reservoir carbonates of the Devonian Nisku Formation, Alberta, Canada: an ion microprobe study. *Geochim. Cosmochim. Acta* **60**, 325–336 (1996).
37. Gustafsson, J. et al. Deep microbial colonization during impact-generated hydrothermal circulation at the Lappajärvi impact structure, Finland. *Nat. Commun.* **16**, 8270 (2025).
38. Drake, H. et al. Unprecedented ^{34} S-enrichment of pyrite formed following microbial sulfate reduction in fractured crystalline rocks. *Geobiology* **16**, 556–574 (2018).
39. Sahlstedt, E., Karhu, J. A., Pitkänen, P. & Whitehouse, M. Implications of sulfur isotope fractionation in fracture-filling sulfides in crystalline bedrock, Olkiluoto, Finland. *Appl. Geochem.* **32**, 52–69 (2013).
40. Fritz, P. & Frape, S. K. Saline groundwaters in the Canadian Shield—a first overview. *Chem. Geol.* **36**, 179–190 (1982).
41. Kietäväinen, R. et al. Characterisation and isotopic evolution of saline waters of the Outokumpu Deep Drill Hole, Finland - Implications for water origin and deep terrestrial biosphere. *Appl. Geochem.* **32**, 37–51 (2013).
42. Karlsson, H. R. & Clayton, R. N. Oxygen and hydrogen isotope geochemistry of zeolites. *Geochim. Cosmochim. Acta* **54**, 1369–1386 (1990).
43. Kloppmann, W., Girard, J.-P. & Négrel, P. Exotic stable isotope compositions of saline waters and brines from the crystalline basement. *Chem. Geol.* **184**, 49–70 (2002).
44. Warr, O. et al. The role of low-temperature ^{18}O exchange in the isotopic evolution of deep subsurface fluids. *Chem. Geol.* **561**, 120027 (2021).
45. Chivian, D. et al. Environmental genomics reveals a single-species ecosystem deep within Earth. *Science* **322**, 275–278 (2008).
46. Head, I. M., Jones, D. M. & Larter, S. R. Biological activity in the deep subsurface and the origin of heavy oil. *Nature* **426**, 344–352 (2003).
47. Stolper, D. A. et al. Combined ^{13}C–D and D–D clumping in methane: methods and preliminary results. *Geochim. Cosmochim. Acta* **126**, 169–191 (2014).
48. Douglas, P. M. J. et al. Methane clumped isotopes: progress and potential for a new isotopic tracer. *Org. Geochem.* **113**, 262–282 (2017).
49. Wang, D. T. et al. Nonequilibrium clumped isotope signals in microbial methane. *Science* **348**, 428–431 (2015).
50. Lorenz, H. et al. COSC-2 – drilling the basal décollement and underlying margin of palaeocontinent Baltica in the Paleozoic Caledonide Orogen of Scandinavia. *Sci. Drill.* **30**, 43–57 (2022).
51. Wu, X. et al. Crustal faulting drives biological redox cycling in the deep subsurface. *Sci. Adv*. **11**, eadx5372 (2025).
52. Parkes, R. J. et al. Rock-crushing derived hydrogen directly supports a methanogenic community: significance for the deep biosphere. *Environ. Microbiol. Rep.* **11**, 165–172 (2019).
53. Zhang, Y. et al. Geological activity shapes the microbiome in deep-subsurface aquifers by advection. *Proc. Natl. Acad. Sci.* **119**, e2113985119 (2022).
54. Huigen, Y. & Andriessen, P. Thermal effects of Caledonian foreland basin formation, based on fission track analyses applied on basement rocks in central Sweden. *Phys. Chem. Earth Parts A/B/C.* **29**, 683–694 (2004).
55. Torsvik, T. H., Sturt, B. A., Swensson, E., Andersen, T. B. & Dewey, J. F. Palaeomagnetic dating of fault rocks: evidence for Permian and Mesozoic movements and brittle deformation along the extensional Dalsfjord Fault, western Norway. *Geophys. J. Int.* **109**, 565–580 (1992).
56. Ksienzyk, A. K. et al. Post-Caledonian brittle deformation in the Bergen area, West Norway: results from K–Ar illite fault gouge dating. *Nor. J. Geol.* **96**, 275–299 (2016).
57. Lehnert, O. et al. The COSC-2 drill core and its well-preserved lower Palaeozoic sedimentary succession—an unexpected treasure beneath the Caledonian nappes. *Est. J. Earth Sci.* **73**, 134–140 (2024).
58. Andersson, A., Claesson, S. & Kooijman, E. Age and crustal affinity of Precambrian basement nappes and underlying basement in the east central Scandinavian Caledonides. (*Geologiska Föreningen Special Publication,* 2022).
59. Lescoutre, R. et al. Large-scale, flat-lying mafic intrusions in the Baltican crust and their influence on basement deformation during the Caledonian orogeny. *GSA Bull.* **134**, 3022–3048 (2022).
60. Gorbatschev, R., Solyom, Z. & Johansson, I. The Central Scandinavian Dolerite Group in Jämtland, central Sweden. *Geol. F.öreningen i Stockh. F.örhandlingar* **101**, 177–190 (1979).
61. Faleide, J. I. et al. Structure and evolution of the continental margin off Norway and the Barents Sea. *Episodes* **31**, 82–91 (2008).
62. Kahraman, M. et al. Northern Scandinavian mountains supported by a low-grade eclogitic crustal keel. *Nat. Commun.* **16**, 606 (2025).
63. Regenspurg, S. et al. Geochemical properties of saline geothermal fluids from the in-situ geothermal laboratory Groß Schönebeck (Germany). *Geochemistry* **70**, 3–12 (2010).
64. Feldbusch, E., Wiersberg, T., Zimmer, M. & Regenspurg, S. Origin of gases from the geothermal reservoir Groß Schönebeck (North German Basin). *Geothermics* **71**, 357–368 (2018).
65. Ono, S. et al. Measurement of a doubly substituted methane isotopologue, $^{13}CH_3D$, by tunable infrared laser direct absorption spectroscopy. *Anal. Chem.* **86**, 6487–6494 (2014).
66. Eldridge, D. L. et al. Comparison of experimental vs theoretical abundances of $^{13}CH_3D$ and $^{12}CH_2D_2$ for isotopically equilibrated systems from 1 to 500 °C. *ACS Earth Space Chem.* **3**, 2747–2764 (2019).
67. Drake, H. et al. Extreme ^{13}C depletion of carbonates formed during oxidation of biogenic methane in fractured granite. *Nat. Commun.* **6**, 1–9 (2015).
68. Ding, T. et al. Calibrated sulfur isotope abundance ratios of three IAEA sulfur isotope reference materials and V-CDT with a reassessment of

the atomic weight of sulfur. *Geochim. Cosmochim. Acta* **65**, 2433–2437 (2001).
69. Roberts, N. M. W. et al. A calcite reference material for LA-ICP-MS U-Pb geochronology. *Geochem., Geophys. Geosyst.* **18**, 2807–2814 (2017).
70. Guillong, M. et al. Technical note: RA138 calcite U–Pb LA-ICP-MS primary reference material. *Geochronology* **6**, 465–474 (2024).
71. Hill, C. A., Polyak, V. J., Asmerom, Y. & Provencio, P. Constraints on a Late Cretaceous uplift, denudation, and incision of the Grand Canyon region, southwestern Colorado Plateau, USA, from U-Pb dating of lacustrine limestone. *Tectonics* **35**, 896–906 (2016).
72. Bernasconi, S. M. et al. InterCarb: a community effort to improve interlaboratory standardization of the carbonate clumped isotope thermometer using carbonate standards. *Geochem. Geophys. Geosyst.* **22**, 1–25 (2021).
73. Dennis, K. J., Affek, H. P., Passey, B. H., Schrag, D. P. & Eiler, J. M. Defining an absolute reference frame for 'clumped' isotope studies of CO_2. *Geochim. Cosmochim. Acta* **75**, 7117–7131 (2011).
74. Daëron, M. Full propagation of analytical uncertainties in Δ_{47} measurements. *Geochem. Geophys. Geosyst.* **22**, 1–19 (2021).
75. Yanay, N. et al. Rapid and precise measurement of carbonate clumped isotopes using laser spectroscopy. *Sci. Adv.* **8**, 611 (2022).
76. Roberts, N. M. W. & Walker, R. J. U-Pb geochronology of calcite-mineralized faults: absolute timing of rift-related fault events on the northeast Atlantic margin. *Geology* **44**, 531–534 (2016).
77. Wang, Z. et al. Rapid and precise analysis of carbon dioxide clumped isotopic composition by tunable infrared laser differential spectroscopy. *Anal. Chem.* **92**, 2034–2042 (2020).
78. Korja, T., Smirnov, M., Pedersen, L. B. & Gharibi, M. Structure of the Central Scandinavian Caledonides and the underlying Precambrian basement, new constraints from magnetotellurics. *Geophys. J. Int.* **175**, 55–69 (2008).
79. Karis, L., 1998: Jämtlands östliga fjällberggrund. In L. Karis & A.G.B. Strömberg (eds.): Beskrivning till berggrundskartan över Jämtlands län. Del 2: Fjälldelen, 1–184. Sveriges geologiska undersökning Ca 53:2. 363 pp. [In Swedish with English summary].
80. Milkov, A. V. & Etiope, G. Revised genetic diagrams for natural gases based on a global dataset of >20,000 samples. *Org. Geochem.* **125**, 109–120 (2018).
81. Miettinen, H. et al. Microbiome composition and geochemical characteristics of deep subsurface high-pressure environment, Pyhäsalmi mine, Finland. *Front. Microbiol.* **6**, 1203 (2015).
82. Kietäväinen, R., Ahonen, L., Niinikoski, P., Nykänen, H. & Kukkonen, I. T. Abiotic and biotic controls on methane formation down to 2.5 km depth within the Precambrian Fennoscandian Shield. *Geochim. Cosmochim. Acta* **202**, 124–145 (2017).
83. Pitkänen, P. & Partamies, S. *Origin and Implications of Dissolved Gases in Groundwater at Olkiluoto* (Posiva Oy, 2007).
84. Gimeno, M. J., Tullborg, E.-L., Nilsson, A.-C., Auqué, L. F. & Nilsson, L. Hydrogeochemical characterisation of the groundwater in the crystalline basement of Forsmark, the selected area for the geological nuclear repositories in Sweden. *J. Hydrol.* **624**, 1–21 (2023).
85. van Dam, F. et al. Microbial methanogenesis fueled by freshwater infiltration and oil biodegradation in the Siljan impact structure, Sweden. *Discov. Appl. Sci.* **7**, 51 (2025).
86. Lollar, G. S., Warr, O., Telling, J., Osburn, M. R. & Lollar, B. S. 'Follow the water': hydrogeochemical constraints on microbial investigations 2.4 km below surface at the Kidd Creek Deep Fluid and Deep Life Observatory. *Geomicrobiol. J.* **36**, 859–872 (2019).
87. Warr, O. et al. Tracing ancient hydrogeological fracture network age and compartmentalisation using noble gases. *Geochim. Cosmochim. Acta* **222**, 340–362 (2018).
88. Li, L. et al. Sulfur mass-independent fractionation in subsurface fracture waters indicates a long-standing sulfur cycle in Precambrian rocks. *Nat. Commun.* **7**, 13252 (2016).
89. Onstott, T. C. et al. The origin and age of biogeochemical trends in deep fracture water of the Witwatersrand Basin, South Africa. *Geomicrobiol. J.* **23**, 369–414 (2006).
90. Nisson, D. M. et al. Hydrogeochemical and isotopic signatures elucidate deep subsurface hypersaline brine formation through radiolysis-driven water-rock interaction. *Geochim. Cosmochim. Acta* **340**, 65–84 (2023).
91. Gimeno, M. J., Auqué, L. F., Gómez, J. B. & Acero, P. *Water-Rock Interaction Modelling and Uncertainties of Mixing Modelling SDM-Site Forsmark*. *CM Gruppen AB* www.skb.se. (2008).
92. Craig, H. Isotopic variations in meteoric waters. *Science* **133**, 1702–1703 (1961).

Acknowledgements

Thanks are due to H. Rothe & S. Tonn, German Centre for Geosciences (GFZ), A. Pullinen and M. Tiljander, Geological Survey of Finland (GTK), T. Vaahtojärvi, University of Helsinki, H. Lorenz, Uppsala University, for their support in the sampling and analysis. This is contribution #51 from the Environmental and Mineralogical Laboratories (Hellabs) of the Department of Geosciences and Geography, University of Helsinki. This is NordSIMS publication #833.

Author contributions

F.vD.: fieldwork, investigation, analysis, visualization, writing – original draft, writing – review & editing, data curation. R.K.: fieldwork, investigation, analysis, methodology, supervision, writing – review & editing. G.W.: fieldwork, investigation, writing – review & editing, data curation. N.M.W.R.: formal analysis, writing – review & editing. Z.W.: formal analysis, writing – review & editing. J.Q.: formal analysis, writing – review & editing. M.J.W.: formal analysis, writing – review & editing. S.O.: formal analysis, writing – review & editing. T.W.: formal analysis, investigation, fieldwork, writing – review & editing. M.D.: conceptualization, resources, supervision, writing – review & editing. H.D.: conceptualization, fieldwork, investigation, formal analysis, writing – review & editing, resources, supervision.

Funding:

COSC-2 was supported and funded by the International Continental Scientific Drilling Program (ICDP) and the Swedish Research Council. The study was supported by a Swedish Research Council Formas grant to H.D. and M.D. (2020-01577); Swedish Research Council grants to H.D. (2021-04365) and M.D. (2024-04607); a J. Gust. Richert foundation grant (to H.D.); a Crafoord Foundation grant to H.D. (20210524); a NSF FRES SMRFS grant to H.D. (EAR 2120733). Open access funding provided by Linnaeus University.

Competing interests

The authors declare no competing interests.

Additional information

Supplementary information The online version contains supplementary material available at https://doi.org/10.1038/s43247-026-04000-1.

Correspondence and requests for materials should be addressed to Femke van Dam.

Peer review information *Communications Earth & Environment* thanks Austin Boyd and the other, anonymous, reviewer(s) for their contribution to the peer review of this work. Primary Handling Editors: Yuan Shang and Alireza Bahadori. A peer review file is available.

Reprints and permissions information is available at http://www.nature.com/reprints

Publisher's note Springer Nature remains neutral with regard to jurisdictional claims in published maps and institutional affiliations.

Open Access This article is licensed under a Creative Commons Attribution 4.0 International License, which permits use, sharing, adaptation, distribution and reproduction in any medium or format, as long as you give appropriate credit to the original author(s) and the source, provide a link to the Creative Commons licence, and indicate if changes were made. The images or other third party material in this article are included in the article's Creative Commons licence, unless indicated otherwise in a credit line to the material. If material is not included in the article's Creative Commons licence and your intended use is not permitted by statutory regulation or exceeds the permitted use, you will need to obtain permission directly from the copyright holder. To view a copy of this licence, visit http://creativecommons.org/licenses/by/4.0/.

© The Author(s) 2026